Taylor & Francis
Taylor & Francis Group

Particulate Science and Technology

An International Journal

ISSN: (Print) (Online) Journal homepage: https://www.tandfonline.com/loi/upst20

Synthesis and characterization of 2-mercaptoethanol-capped manganese-doped zinc sulfide quantum dots-embedded molecularly-imprinted membranes

Hui Ying Thor, Yeit Haan Teow & Kah Chun Ho

To cite this article: Hui Ying Thor, Yeit Haan Teow & Kah Chun Ho (2021): Synthesis and characterization of 2-mercaptoethanol-capped manganese-doped zinc sulfide quantum dots-embedded molecularly-imprinted membranes, Particulate Science and Technology, DOI: 10.1080/02726351.2021.1903634

To link to this article: https://doi.org/10.1080/02726351.2021.1903634

PARTICULATE SCIENCE AND TECHNOLOGY
https://doi.org/10.1080/02726351.2021.1903634

Synthesis and characterization of 2-mercaptoethanol-capped manganese-doped zinc sulfide quantum dots-embedded molecularly-imprinted membranes

Hui Ying Thor[a], Yeit Haan Teow[a,b], and Kah Chun Ho[a,c]

[a]Department of Chemical and Process Engineering, Faculty of Engineering and Built Environment, Universiti Kebangsaan Malaysia, Bangi, Selangor Darul Ehsan, Malaysia; [b]Research Centre of Sustainable Process Technology (CESPRO), Faculty of Engineering and Built Environment, Universiti Kebangsaan Malaysia, Bangi, Selangor Darul Ehsan, Malaysia; [c]Faculty of Engineering, Built Environment, and Information Technology, SEGi University, Kota Damansara, Selangor Darul Ehsan, Malaysia

ABSTRACT

The objective of this study is to synthesize QD-embedded molecularly imprinted membranes (MIMs) with 2-mercaptoethanol-capped manganese-doped zinc sulfide quantum dots (ME-capped Mn-doped ZnS QDs) through chemical precipitation followed by surface molecular imprinting. For the synthesis of the MIMs, the weight of ME-capped Mn-doped ZnS QDs was first manipulated, followed by their characterization through transmission electron microscopy (TEM), zeta potential, hydrodynamic particle size, particle size distribution, and Fourier-transform infrared spectroscopy (FTIR). The resultant MIM was characterized by fluorescence intensity and showed an emission peak of 600 nm with an excitation wavelength of 300 nm. Besides, increments in QDs were found to elevate the fluorescence intensity of the MIM, contributing to an improved fluorescence quantum yield. This article indicates that molecularly-imprinted QD-based sensors offer promising biomedical potential in diagnoses and treatment.

KEYWORDS

Quantum dots; molecular imprinted; biosensor; fluorescence

1. Introduction

Over the last decade, quantum dots (QDs) have been hailed as the most promising nanoparticles, given their numerous advantages. In analyte detection and biosensor development, the fluorescence-quenching effect of QDs due to electron transfer between the QDs and the target molecule makes them a favorable choice (Chen et al. 2014). Furthermore, QDs possess unique benefits including established excellent stability, high fluorescence quantum yield, and adjustable size-dependent fluorescent emission (Bakar et al. 2010, 2011; Li et al. 2010; Shamsudin and Junas 2018; Abu Bakar, Ali Umar, and Mat Salleh 2019). QDs are resistant to photobleaching and able to give bright fluorescence after a repetitive cycle of excitation (Li 2008; Borse et al. 2018). Their higher fluorescence quantum yield gives a brighter fluorophore and thus stronger fluorescence intensity signal that could more easily be detected and quantified. Besides, optical and conducting properties of the QDs can be controlled given their size-tunable wavelength (Wang et al. 2017). Zinc sulfide (ZnS) QDs are the most commonly-studied QDs for biological applications due to the wide band gap value of 3.54 eV and easily tunable fluorescent emission in the visible range (Amran and Shamsudin 2016; Kuznetsova, Kazantseva, and Rempel 2016). Recently, a photoelectrochemical biosensor for detecting uric acid was developed by Raheem and Olowu (2013) based on ZnS nanostructures-based electrochemical biosensor. By depositing the ZnS on a working electrode, they found that the electrodes demonstrated better sensitivity in detection than nanoparticles because of their higher surface-area-to-volume ratio.

Doping of the QDs with transition metal atoms has been found to modify their band gap and photoluminescent properties due to size changes (Shamsudin and Junas 2018). Doping introduces steric hindrance and enhances electrostatic stabilization, thus enabling the formation of small-sized nanoparticles (Murugadoss and Ramasamy 2012). Dopants, such as manganese (Mn) have attracted substantial scholarly interest because of their paramagnetic properties that enhance the magnetic and optical features of the QDs. Kole and Kumbhakar (2012) reported that the doping of Mn^{2+} in increasing concentrations improved photoluminescence due to the particle size-dependent crystal field effect and the surface effects. Mn-doped ZnS thus exhibited better multi-photon absorptive characteristics and a wider direct band gap (5.6 eV) than pristine ZnS (3.71 eV).Furthermore, the addition of a capping agent in the QDs has been proposed to not only stabilize and passivate their surfaces to obtain desirable optical properties, but also to control their growth (Pradeep et al. 2017). In this regard, mercaptoethanol (ME), a reducing agent, has been widely used as a capping agent to prevent agglomeration due to the instability of semiconductors (Masab et al. 2018). For ZnS, the capping of ME has been shown to have superior band gap energy

CONTACT Yeit Haan Teow yh_teow@ukm.edu.my Department of Chemical and Process Engineering, Faculty of Engineering and Built Environment, Universiti Kebangsaan Malaysia, Bangi, Selangor Darul Ehsan, Malaysia.

(4.23 eV), compared to other agents, such as thiourea (3.85 eV) and L-cysteine (3.92 eV) (Rajabi and Farsi 2016). In accordance to quantum confinement effects, the band gap energy increases with decreasing sizes of the QDs (Mustakim et al. 2020). A larger band gap energy causes more time for electron-hole recombination, resulting in a higher photocatalytic activity (Behnajady and Tohidi 2014).

Despite its performance in specific recognition, traditional molecular imprinting suffers from the drawback of lacking signal outputs during analysis (Liu et al. 2019). Therefore, QDs are commonly integrated with molecular imprinting techniques to realize specific recognition and fluorescence detection as a biosensor. Recently, Zhang et al. (2018) prepared a fluorescent molecularly-imprinted membrane (MIM) by embedding L-cysteine-capped Mn^{2+}-doped ZnS QDs into a molecularly imprinted polymer matrix. The MIM was applied to determine lysozyme in real samples with recoveries of 93–103%. Besides, the concentration of QDs in a MIM is known to crucially affect both fluorescence intensity and quenching efficiency. Wang et al. (2019) reported that a narrow linear range of quenching efficiency produced from cadmium telluride (CdTe) QDs at low concentrations (30–80 μ g/mL) and low sensitivity through high concentrations (above 100 μ g/mL). This was attributed to the slight agglomeration of CdTe QDs at higher concentrations. However, fluorescence is believed to vary depending on the type of QDs used in Mims. In this article, ME-capped Mn-doped ZnS QDs were synthesized through co-precipitation, given its simplicity and rapidity compared to other techniques such as microwave-assisted synthesis. Additionally, co-precipitation required no expensive equipment and the crystalline structure of QDs could be easily monitored from the reaction temperature and atmosphere. Following this, the ME-capped Mn-doped ZnS QD-embedded MIM was synthesized through surface molecular imprinting, during which the weight of ME-capped Mn-doped ZnS QDs was manipulated. The performance of the synthesized MIM was characterized by its fluorescence. The application of QDs in optical sensors has garnered much attention due to their extraordinary optical and electronic properties (Wang et al. 2017). The application of molecular imprinting on QDs presents a new form of fluorescence-based MIMs for the development of fluorescence optical sensors as a diagnostic kit in the biomedical field (Wang et al. 2019). Such MIMs are envisioned to increase the diagnostic efficiency while reducing operational costs.

2. Experimental details

2.1. Materials

ME (purity ≥99%), N,N'-methylenediacrylamide (BIS) (purity ≥99%), and N,N,N′,N′-tetramethylethylenediamine (TEMED) (purity ≥99%) were purchased from Solarbio, China. Zinc nitrate, Mn (II) acetate tetrahydrate, acrylamide monomer (purity: 99.5%), ammonium persulphate, monosodium phosphate, disodium phosphate, and acetic acid were supplied by R&M-Chemicals, Malaysia. Sodium sulfide was obtained from Alfa Aesar, US. Sodium dodecyl sulfate (SDS) and isopropyl alcohol were purchased from Chemiz, Malaysia and HmbG-Chemicals, Malaysia, respectively.

2.2. Synthesis of ME-capped Mn-doped ZnS QDs

ME-capped Mn-doped ZnS QDs were synthesized through chemical precipitation (Pradeep et al. 2017). About 50 mL of 0.1 M ME was added dropwise into a three-necked flask containing 50 mL of 0.1 M zinc nitrate and 50 mL of 0.008 M Mn (II) acetate tetrahydrate at room temperature. The flask was purged with inert nitrogen gas and continuously stirred at 250 rpm for 30 min. Next, 50 mL of 0.1 M sodium sulfide was added dropwise into the mixture to allow the nucleation of QDs. Stirring was allowed to continue for 1 h at room temperature in the dark for the formation of ME-capped Mn-doped ZnS QDs, followed by centrifuging the mixture at 11,000 rpm for 15 min. The resultant precipitate was washed three times with ultrapure water and 30 *v/v*% isopropyl alcohol and then dried in a vacuum oven at 100 °C for 2 h. The synthesized ME-capped Mn-doped ZnS QDs (in powder form) were then transferred into a clean brown reagent bottle, sealed, and stored in refrigerator at 4 °C for subsequent use.

2.3. Synthesis of ME-capped Mn-doped ZnS QDs embedded MIM

The ME-capped Mn-doped ZnS QD-embedded MIM was synthesized through surface molecular imprinting (Zhang et al. 2018). First, 240 mg of acrylamide monomer and 0.3 mL of pre-determined lysozyme (0–20 mg/mL) were dissolved in 2 mL of 0.02 M PBS at pH 6.4 (Zhang et al. 2018). The mixture was sonicated in an ultrasonicator, WUC-A03H (Daihan Sci, Seoul, Korea) at 40 kHz for 20 min. About 1 mL of 10 mg/mL BIS and various weights (10–20 mg) of the synthesized ME-capped Mn-doped ZnS QDs were then added into the mixture (Zhang et al. 2016). It was further subjected to stirring for 30 min, deoxygenation with nitrogen purge for 5 min to promote polymerization, and then sonication for another 30 min. Subsequently, 40 μL of ammonium persulphate (10 *w/w*%) and 5 µL of TEMED were added to the mixture. The resultant polymeric mixture was dropped into a glass mold (2 cm × 2 cm) under a nitrogen-filled atmosphere and then left to dry at room temperature for 12 h. The ME-capped Mn-doped ZnS QD-embedded MIM was washed repeatedly with a mixture of SDS (10 *w/v*%) and acetic acid (10 *v/v*%) to remove any remaining chemicals on its surface. The formulation of ME-capped Mn-doped ZnS QD-embedded MIM is outlined in Table 1.

Table 1. Formulation of ME-capped Mn-doped ZnS QDs embedded MIM.

ME-capped Mn-doped ZnS QDs embedded MIM	Weight of QDs (mg)
M0A	10
M0B	15
M0C	20

2.4. Characterization of ME-capped Mn-doped ZnS QDs

2.4.1. Transmission electron microscopy (TEM)

TEM Talos L120C (Thermo Fisher Scientific, Waltham, MA, USA) with an accelerating voltage of 200 kV was used to observe the structure of the synthesized ME-capped Mn-doped ZnS QDs. The QD suspension was dispersed in ethanol and sonicated for 30 min prior to TEM analysis. The mixture was then dropped onto copper grids covered with holey carbon films. The droplet was air-dried and subjected to TEM imaging under 120 k × and 310 k × magnification.

2.4.2. Zeta potential

The stability of ME-capped Mn-doped ZnS QDs in PBS was indicated by the zeta potential of the suspension, measured through Zeta Sizer Nano-ZS (Malvern Instrument Inc., Malvern, UK). Zeta Sizer Nano-ZS was equipped with a HeSe laser operating at the wavelength of 633 nm and a scattering detector at 173°. In general, a given nanoparticle suspension with a zeta potential greater than +30 mV or less than −30 mV is considered to exhibit stability (Kumar and Dixit 2017).

2.4.3. Hydrodynamic particle size and particle size distribution

The hydrodynamic particle size and particle size distribution of ME-capped Mn-doped ZnS QDs were measured through the Zeta Sizer Nano-ZS (Malvern Instrument Inc., Malvern, UK). A suspension was prepared by dispersing the QDs in PBS and sonicated for 30 min prior to the analysis at concentration of 1 g/L. The dispersed QDs suspension was placed in 1 cm path-length quartz cell and analyzed by Zeta Sizer Nano-ZS. The particle size and particle size distribution were measured in triplicates, of which the average value was reported.

2.4.4. Fourier transform infrared (FTIR)

FTIR spectroscopy, Nicolet 6700 (Thermo Fisher Scientific Inc., Waltham, MA, USA), was used to examine the functional groups present on the synthesized ME-capped Mn-doped ZnS QDs. The FTIR spectroscopy was equipped with a diamond crystal operating under the attenuated total reflectance (ATR) mode with wavenumbers ranging between 400 and 4000 cm^{-1}. Equal pressure was applied for each sample to avoid analytical errors.

2.5. Characterization of ME-capped Mn-doped ZnS QDs embedded MIM

2.5.1. Fluorescence intensity

The fluorescence intensity of the synthesized ME-capped Mn-doped ZnS QD-embedded MIM was measured through FLS920 fluorescence spectrometer (Edinburgh Instruments Ltd, Livingston, UK) with wavelengths ranging between 220 and 750 nm under ambient conditions. The excitation wavelength was set to be 300 nm (Wang et al. 2017).

3. Results and discussion

3.1. Characterization of ME-capped Mn-doped ZnS QDs

Under 310 k × magnification, TEM imaging reveals agglomeration of the ME-capped Mn-doped ZnS QDs due to solvent evaporation (Figure 1(a)); such clustering could be attributed to strong intermolecular Van der Waals forces between the QDs (Mao et al. 2016). Under 120 k × magnification, TEM imaging reveals the particle size of the ME-capped Mn-doped ZnS QDs to be in the range of 2.2–3.4 nm (Figure 1(b)): these were slightly smaller than those synthesized through the same method by Pradeep et al. (2017), reported to be in the range of 2.5–2.9 nm. Doping of capping agents onto the ZnS QDs was found to decrease their particle size. This could be explained by the two-step growth process of the QDs: Ostwald ripening and

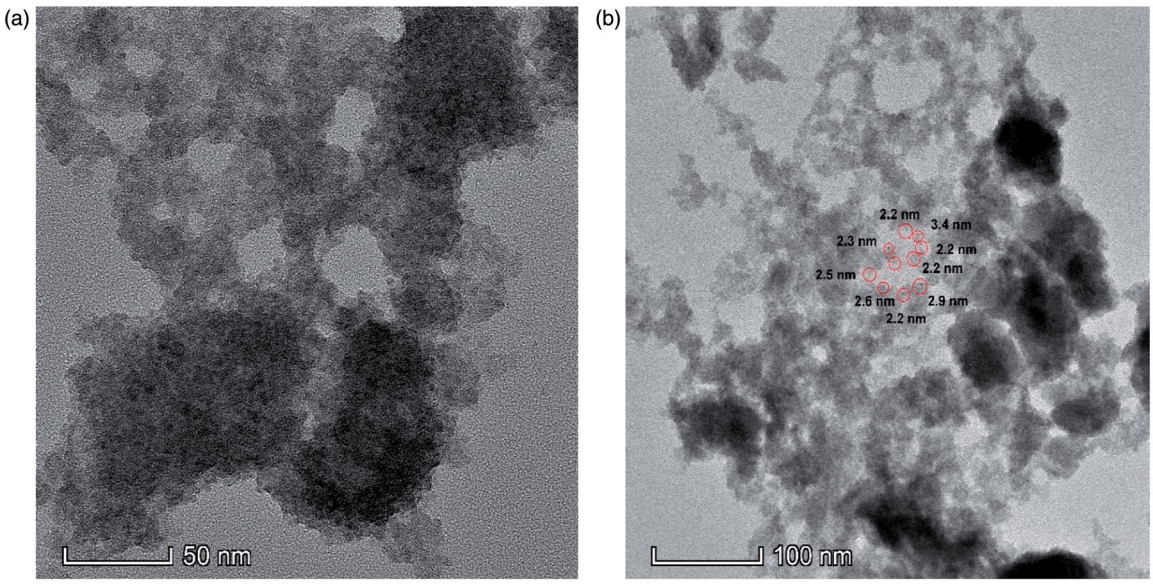

Figure 1. TEM images of ME capped Mn-doped ZnS under (a) 310 k × magnification (b) 120 k × magnification.

oriented attachment (Masab et al. 2018). Direct modification onto the surface of the QDs by capping agents would affect the oriented attachment. The presence of such agents promoted surface passivation of the QDs and suppressed their growth, thus resulting in quantum confinement (Rajabi and Farsi 2016). The resultant confinement of carriers in the core thereby reduced their particle size (Neikov and Yefimov 2019). With the diminution of the QD size, the band gap migrates from the near-infrared range into the visible range: this would be useful since environmental remediation relies on the sun as the light source (Teow et al. 2018). Another result from the diminution of the QD size is the larger surface areas and unique optical properties: these would be useful for various biomedical applications owing to their quantum size effect (Chua et al. 2021).

Table 2 summarizes the zeta potential measurement of the ME-capped Mn-doped ZnS QDs, for which the average value in PBS at pH 6.4 was −37.1 mV. The negative sign of the zeta potential reflected the dense electron cloud concentrating on the QDs while the value of zeta potential relied upon the short- or long-term stability of QDs. The high negative zeta potential value of ME-capped Mn-doped ZnS QDs enabled good colloidal stability between particles in a suspension. Based on the Gouy–Chapman–Stern model of electrical double layer theory, two layers of charges surrounded the ME-capped Mn-doped ZnS QDs (Fatehah, Aziz, and Stoll 2014): the first was the compact layer of zinc ion (Zn^{2+}) and sulfide ion (S^{2-}), while the second was the loosely-attached diffuse layer of Zn^{2+} ions into S^{2-} containing medium. The zeta potential of the QDs was attributed to the potential difference between the compact layer and bulk solution across the diffuse layer (Riaz et al. 2018). Besides, such zeta potential can be potentially useful in selectively adsorbing charged molecules in the sensor/biosensor design.

Table 2. Zeta potential of ME-capped Mn-doped ZnS QDs.

Run	Zeta potential (mV)
1	−35.9
2	−37.9
3	−37.5

Figure 2 shows the particle size distribution of ME-capped Mn-doped ZnS QDs in PBS at pH 6.4. Their mean particle size was calculated to be 787.1 nm; however, the range of the particle size distribution was huge. The reason was that the dispersion of the QDs up to single-particle size was forbidden due to the strong attractive forces between the particles as evidenced by the TEM images (Figure 1). ME-capped Mn-doped ZnS QDs were attached in aggregates because of Brownian motion and formed solid bridging with adjacent particles (Akbari, Tavandashti, and Zandrahimi 2011; Uma et al. 2011). Moreover, dynamic light scattering was more sensitive to the presence of large particles (particle larger than 3 nm) as they would dominate the scattering of the light thus detected (Kumar, Singhal, and Sharma 2013). Therefore, the measurement of single-particle size QDs with the use of TEM analysis would be more accurate.

Figure 3 shows the FTIR spectrum of ME and ME-capped Mn-doped ZnS. Upon capping, the absorption band of the –SH group at 2557 cm^{-1} for ME disappeared, as attributed to the cleavage of S–H bond and formation of the new covalent bond between the –SH group and ZnS QDs (Kuznetsova, Kazantseva, and Rempel 2016). This disappearance further confirmed the assembly of ME onto the surface of the ZnS QDs. The peak at 1004 cm^{-1} for the ME-capped Mn-doped ZnS verified the presence of resonance between S-ions in the ZnS crystal (Pradeep et al. 2017). On the other hand, sharp peaks observed at 1056 and 1233 cm^{-1} corresponded to the asymmetric C–O stretching vibrational mode, reflecting the surface modification of ME by ZnS passivation (Kumar, Singhal, and Sharma 2013; Kaur, Sharma, and Pandey 2015). These spectral findings (Figure 3) collectively concluded the successful synthesis of the ME-capped Mn-doped ZnS QDs through co-precipitation.

In the optical characterization of QDs, photoluminescence spectroscopy offered valuable utility with its rapid responses. Under visible light, the color of ME-capped Mn-doped ZnS QDs dispersed in 0.02 M PBS presented a milky coloration. However, under UV light at 265 nm, such QDs changed from white to orange, as attributed to the 4T1→6A1 triplet transition of Mn^{2+} dopant when exposed to UV light (Wu et al. 2014). Such a fluorescence turn-on assay approach has been reported for determining analyte

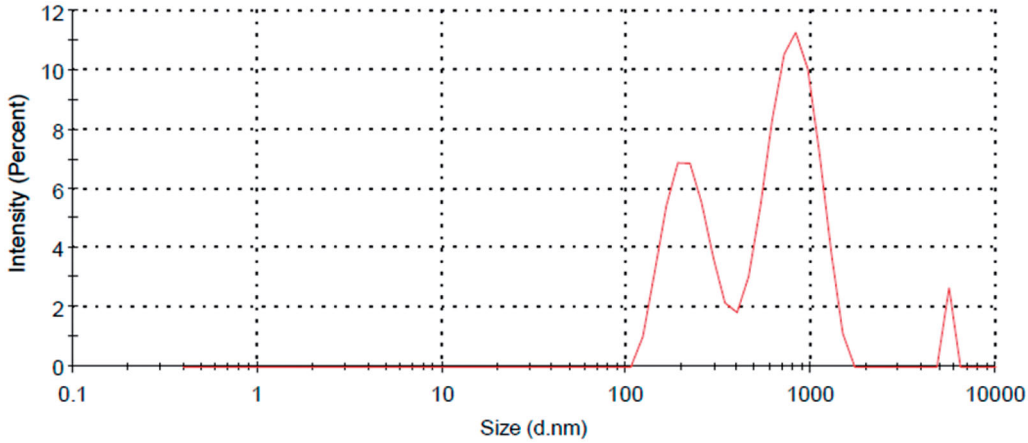

Figure 2. Particle size distribution of ME-capped Mn-doped ZnS QDs in PBS at pH 6.4.

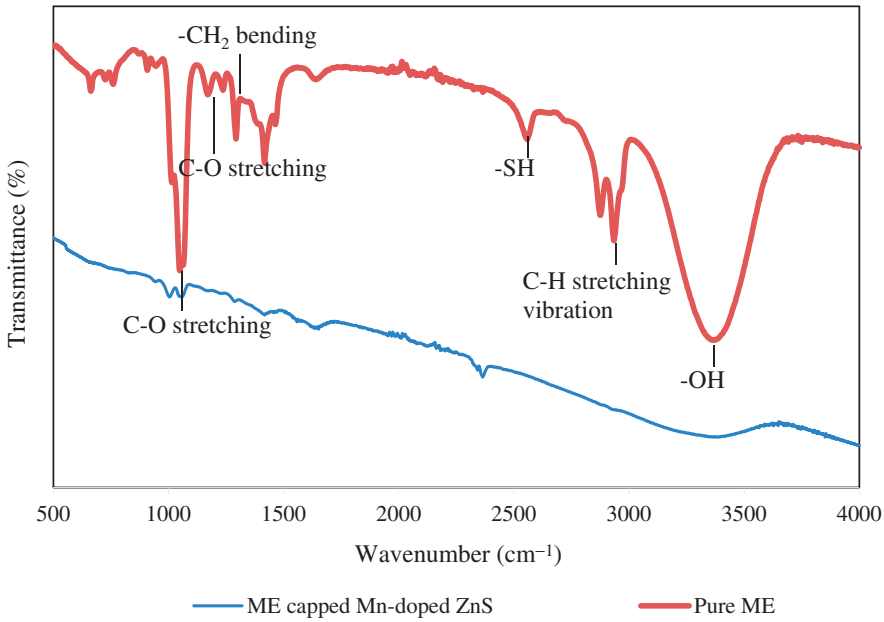

Figure 3. FTIR spectra of ME and ME capped Mn-doped ZnS.

Table 3. ZnS QDs synthesized by different methods.

Method	QDs/Nanoparticles	Color	Size (nm)	Shape	Structure	Reference
Co-precipitation	ME-capped Mn-doped ZnS	Bright orange under excitation wavelength 300 nm	2.3–3.0	Spherical	–	This study
Co-precipitation	L-cysteine capped Mn-doped ZnS	Bright orange under excitation wavelength 265 nm	3.0–4.0	Spherical	Zinc blende	Zhang et al. (2016)
Co-precipitation	ME-capped ZnS	–	2.2–2.8	Spherical	Zinc blende	Pradeep et al. (2017)
	Chitosan capped ZnS	–	2.5–2.8	Spherical	Zinc blende	
	ZnS	–	3.0	Spherical	Zinc blende	
	ME-capped Mn-doped ZnS	–	2.0	Spherical	Zinc blende	
Co-precipitation	ZnS	Blue under excitation wavelength 280 nm	7.0–9.0	Fine fibrous	Zinc blende	Pathak et al. (2012)
Thermal decomposition	ZnS	–	6.0 – 11.0	Rough spherical	Hexagonal wurtzite	Abdullah et al. (2016)
Microwave-assisted synthesis	Mn-doped ZnS	Orange under excitation wavelength 254 nm	5.0–9.0 (triangular), 12.0–14.0 (cubic)	Triangular and cubic	Zinc blende	Sousa et al. (2018)
Microwave-activated synthesis	Mn-doped ZnS	Orange under excitation wavelength 254 nm	3.3	–	Zinc blende	Marandi et al. (2011)
Inverse micelle	Mn-doped ZnS	Yellow-orange under excitation wavelength 318 nm	3.0–5.0	Spherical	Zinc blende	Murugadoss (2011)

concentrations as biosensors. For example, Zhao et al. (2016) established a label-free technique, with graphene QDs as effective probes for the quantification of dopamine: the QDs yielded a strong blue fluorescence in the aqueous solution, which was then quenched by adding dopamine.

Table 3 summarizes the characteristics of ZnS QDs synthesized by various wet chemical methods with or without capping agents or dopants. An observation is that the size of ZnS QDs after capping/doping is smaller than the ZnS QDs, as is in accordance with the findings reported herein. Besides, the distinction between the various fluorescence colors emitted by the ZnS QDs synthesized through the different methods could be useful for differentiating any given analytes of interest.

3.2. Characterization of ME-capped Mn-doped ZnS QDs embedded MIM

Figure 4 shows the fluorescence spectra of ME-capped Mn-doped ZnS QDs embedded MIM with different weights of QDs at 10 mg (M0A), 15 mg (M0B), and 20 mg (M0C). The sample was excited at 300 nm through a FLS920 fluorescence spectrometer (Edinburgh Instruments Ltd, UK). Photoluminescence occurred where an electron from the valence band of ZnS became excited and jumped into the conduction band, followed by its decay through recombination to a defect state (Pathak et al. 2012; Kannappan and Dhanasekaran 2019). The fluorescence emission peak at 600 nm verified the emission of orange light by ME-capped Mn-doped ZnS QD-embedded MIM, secondary to the

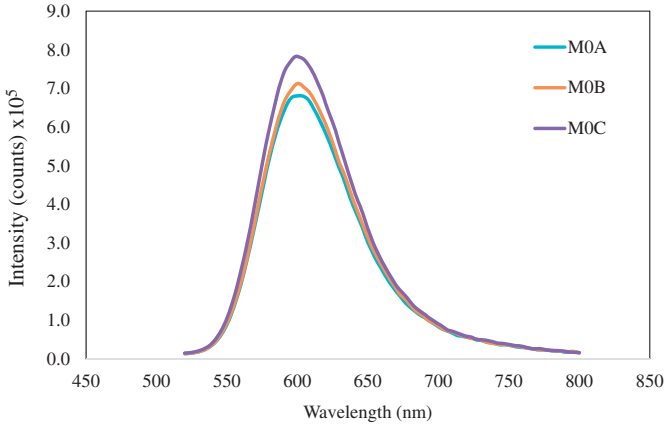

Figure 4. Fluorescence spectra of non-imprinted membrane with different amount of QDs embedded.

photo-excitation of the host ZnS QDs bound with the lower-lying state of Mn^{2+} ions (Kannappan and Dhanasekaran 2019).

A noteworthy observation (Figure 4) has been that fluorescence intensity would increase with the weight of QDs incorporated in the MIM, in the sequence of M0C < M0B < M0A. A greater amount of QDs embedded in the MIM increased the total effective surface area, thereby contributing to a higher quantum yield of fluorescence and a stronger signal intensity. This enhancement would allow for a lower detection limit and improve the sensitivity for fluorescent-based sensing applications.

4. Challenges

Despite the extraordinary fluorescence of QD-embedded MIM, the wide application of molecular imprinting has been hindered by challenges such as proper protein selection, washing method and template removal, and quantification of rebinding (Verheyen et al. 2011). First, during selection, it must be noted that proteins are known for their structural complexity and the presence of many potential recognition sites on their surfaces, such as charged amino acids and hydrophobic or hydrophilic regions (Wang et al. 2019). These could lead to cross-reactivity with and false recognition of proteins with similar charges, hydrophobicity, or hydrophilicity as the imprinted template, thus complicating the synthesis of MIMs with high selectivity. Therefore, future studies should examine such strong interactions, either electrostatic or hydrophobic, between monomers and template that can lead to indiscriminate binding.

Second, for washing and template removal, the combination of acetic acid with a detergent has been the most frequently used; however, this harsh method does not guarantee complete template removal (Ren and Chen 2015). Imprinted templates with a strong binding affinity have been found to retain the template molecules. Besides, specific interactions or protein precipitation by detergent molecules present in the polymer network may lead to false-positive results. Hence, extensive rinsing is warranted for maximized removal of the remainders.

Lastly, in the quantification of template rebinding, template depletion from the solution has commonly been used as a proxy indicator. This method may be deemed unreliable as it does not confirm that the template is bound to the MIM: the apparent template depletion could result from nonspecific binding caused by electrostatic interactions between the template and the MIM. Thus, samples not containing MIM or NIM should be included as an extra control alongside the normal NIM.

5. Conclusion

In conclusion, the synthesis of ME-capped Mn-doped ZnS QDs was performed successfully through co-precipitation. The synthesized QDs exhibited an emission peak of 600 nm in photoluminescence analysis with an excitation wavelength of 300 nm, with the emission light showing bright orange coloration. Doping of Mn and capping with ME successfully yielded QDs of smaller sizes and with better optical properties, in accordance with the quantum confinement effect. TEM and XRD results indicated that the QDs demonstrated the zinc blende structure, whose size ranged between 2.2 and 3.4 nm. FTIR analysis further suggested that the successful capping of ME on the QDs and their controlled growth. Besides, elevating the amount of QD-embedded MIM has been found to contribute to superior fluorescence intensity and fluorescence quantum yield. Future works should evaluate the performance of QD-embedded MIMs on real samples for both detection and quantification. QD-embedded MIM-based sensors offer promising potential in biomedical applications because of their specificity, cost-efficiency, and selectivity with respect to the ease of preparation and versatility for diverse biomolecules.

Disclosure statement

No potential conflict of interest was reported by the author(s).

Funding

This work was financially supported by Infineon Technologies (Kulim) Sdn Bhd [KK-2020-012] and Indah Water Konsortium Sdn Bhd [KK-2018-005].

ORCID

Yeit Haan Teow http://orcid.org/0000-0001-5562-9832
Kah Chun Ho http://orcid.org/0000-0001-5591-3120

References

Abdullah, N. H., Z. Zainal, S. Silong, M. I. M. Tahir, K. B. Tan, and S. K. Chang. 2016. Synthesis of zinc sulphide nanoparticles from thermal decomposition of zinc N-ethyl cyclohexyl dithiocarbamate complex. *Materials Chemistry and Physics* 173:33–41. doi:10.1016/j.matchemphys.2016.01.034.

Abu Bakar, N., A. Ali Umar, and M. Mat Salleh. 2019. Reka bentuk sensor pendar cahaya bintik kuantum ZnCdSe untuk mengesan racun perosak. *Sains Malaysiana* 48 (7):1513–8. doi:10.17576/jsm-2019-4807-20.

Akbari, B., M. P. Tavandashti, and M. Zandrahimi. 2011. Particle size characterization of nanoparticles- a practical approach. *Iranian Journal of Materials Science and Engineering* 8 (2):48–56.

Amran, A. S., and S. A. Shamsudin. 2016. Optical properties of colloidal CdS and ZnS quantum dots nanoparticles. AIP Conference Proceedings, 1784.

Bakar, N. A., A. A. Umar, M. M. Salleh, and M. Yahaya. 2010. Synthesis of CdTe- CdSe core-shell quantum dots with luminescence in the red. *Sains Malaysiana* 39 (3): 473–477.

Bakar, N. A., M. M. Salleh, A. A. Umar, and M. Yahaya. 2011. The detection of pesticides in water using ZnCdSe quantum dot films. *Advances in Natural Sciences: Nanoscience and Nanotechnology* 2 (2):025011. doi:10.1088/2043-6262/2/2/025011.

Behnajady, M. A., and Y. Tohidi. 2014. Synthesis, characterization and photocatalytic activity of Mg-impregnated ZnO-SnO2 coupled nanoparticles. *Photochemistry and Photobiology* 90 (1):51–6. doi:10.1111/php.12164.

Borse, V., A. Kashikar, R. Srivastava, and I. Powai, Indian Institue of Technology Bombay (IIT B) 2018. Fluorescence stability of mercaptopropionic acid capped cadmium telluride quantum dots in various biochemical buffers. *Journal of Nanoscience and Nanotechnology* 18 (4):2582–91. doi:10.1166/jnn.2018.14315.

Chen, H., L. Lin, H. Li, and J.-M. Lin. 2014. Quantum dots-enhanced chemiluminescence: Mechanism and application. *Coordination Chemistry Reviews* 263–264:15–86. doi:10.1016/j.ccr.2013.07.013.

Chua, S. F., A. Nouri, W. L. Ang, E. Mahmoudi, A. W. Mohammad, A. Benamor, and M. Ba-Abbad. 2021. The emergence of multifunctional adsorbents and their role in environmental remediation. *Journal of Environmental Chemical Engineering* 9 (1):104793. doi:10.1016/j.jece.2020.104793.

Fatehah, M. O., H. A. Aziz, and S. Stoll. 2014. Nanoparticle properties, behavior, fate in aquatic systems and characterization methods. *Journal of Colloid Science and Biotechnology* 3 (2):111–40. doi:10.1166/jcsb.2014.1090.

Kannappan, P., and R. Dhanasekaran. 2019. Structural and optical characterization of ZnS nanoparticles synthesized by low temperature solid-state method. *International Journal of Recent Technology and Engineering* 7 (4):26–8.

Kaur, J., M. Sharma, and O. P. Pandey. 2015. Effect of pH on size of ZnS nanoparticles and its application for dye degradation. *Particulate Science and Technology* 33 (2):184–8. doi:10.1080/02726351.2014.952802.

Kole, A. K., and P. Kumbhakar. 2012. Effect of manganese doping on the photoluminescence characteristics of chemically synthesized zinc sulfide nanoparticles. *Applied Nanoscience* 2 (1):15–23. doi:10.1007/s13204-011-0036-x.

Kumar, A., and C. K. Dixit. 2017. *Methods for characterization of nanoparticles.* Advances in nanomedicine for the delivery of therapeutic nucleic acids, 44–58. Amsterdam, Netherlands: Elsevier.

Kumar, S., M. Singhal, and J. K. Sharma. 2013. Functionalization and characterization of ZnS quantum dots using biocompatible l-cysteine. *Journal of Materials Science: Materials in Electronics* 24 (10):3875–80. doi:10.1007/s10854-013-1332-x.

Kuznetsova, Y. V., A. A. Kazantseva, and A. A. Rempel. 2016. Zeta potential, size, and semiconductor properties of zinc sulfide nanoparticles in a stable aqueous colloid solution. *Russian Journal of Physical Chemistry A* 90 (4):864–9. doi:10.1134/S0036024416040154.

Li, H. 2008. Synthesis and characterization of aqueous quantum dots for biomedical application. Synthesis and characterization of aqueous quantum dots for biomedical application. Thesis, Drexel University.

Li, Z., Y. Wang, J. Wang, Z. Tang, J. G. Pounds, and Y. Lin. 2010. Rapid and sensitive detection of protein biomarker using a portable fluorescence biosensor based on quantum dots and a lateral flow test strip. *Analytical Chemistry*, 82 (16):7008–14. doi:10.1021/ac101405a.

Liu, G., X. Huang, L. Li, X. Xu, Y. Zhang, J. Lv, and D. Xu. 2019. Recent advances and perspectives of molecularly imprinted polymer-based fluorescent sensors in food and environment analysis. *Nanomaterials* 9 (7):1030. doi:10.3390/nano9071030.

Mao, Y., M. Meng, L. Yan, F. Sun, Y. Yan, and S. Liu. 2016. Fabrication of highly selective molecularly imprinted membranes for the selective adsorption of methyl salicylate from salicylic acid. *RSC Advances* 6 (94):91659–68. doi:10.1039/c6ra17955j.

Marandi, M., G. Hajisalem, N. Taghavinia, and M. Houshiar. 2011. Fast two-step microwave-activated synthesis of Mn doped ZnS nanocrystals: Comparison of the luminescence and doping process with thermochemical approach. *Journal of Luminescence* 131 (4):721–6. doi:10.1016/j.jlumin.2010.11.025.

Masab, M., H. Muhammad, F. Shah, M. Yasir, and M. Hanif. 2018. Facile synthesis of CdZnS QDs: Effects of different capping agents on the photoluminescence. *Materials Science in Semiconductor Processing* 81:113–7. doi:10.1016/j.mssp.2018.03.023.

Murugadoss, G. 2011. Synthesis, optical, structural and thermal characterization of Mn doped ZnS nanoparticles using reverse micelle method. *Journal of Luminescence* 131 (10):2216–23. doi:10.1016/j.jlumin.2011.03.048.

Murugadoss, G., and V. Ramasamy. 2012. Synthesis, effect of capping agents and optical properties of manganese-doped zinc sulphide nanoparticles. *Luminescence* 28:69–75. doi:10.1002/bio.2346.

Mustakim, N. S. M., J. Safaei, C. A. Ubani, S. Sepeai, N. A. Ludin, M. A. M. Teridie, and M. A. Ibrahim. 2020. Preliminary study of effective copper indium sulfide (CuInS2) quantum dots as photo-sensitizer in solar cell. *Jurnal Kejuruteraan* 32 (2): 307–313.

Neikov, O. D., and N. A. Yefimov. 2019. *Nanopowders. Handbook of nonferrous metal powders*, 271–311. Amsterdam, Netherlands: Elsevier.

Pathak, C. S., D. D. Mishra, V. Agarwala, and M. K. Mandal. 2012. Optical properties of ZnS nanoparticles produced by mechanochemical method. *Ceramics International* 38 (8):6191–5. doi:10.1016/j.ceramint.2012.04.070.

Pradeep, S., S. Raghuram, M. G. Chaudhury, and S. Mazumder. 2017. ynthesis and Characterization of Fe3+ and Mn2+ doped ZnS quantum dots for photocatalytic applications: Effect of 2-mercaptoethanol and chitosan as capping agents. *Journal of Nanoscience and Nanotechnology* 17 (2):1125–32. doi:10.1166/jnn.2017.12599.

Raheem, A. A., and O. A. Olowu. 2013. Production of household paint using clay materials. *International Journal of Engineering Research and Applications* 3 (2):85–93.

Rajabi, H. R., and M. Farsi. 2016. Study of capping agent effect on the structural, optical and photocatalytic properties of zinc sulfide quantum dots. *Materials Science in Semiconductor Processing* 48:14–22. doi:10.1016/j.mssp.2016.02.021.

Ren, X., and L. Chen. 2015. Quantum dots coated with molecularly imprinted polymer as fluorescence probe for detection of cyphenothrin. *Biosensors & Bioelectronics* 64:182–8. doi:10.1016/j.bios.2014.08.086.

Riaz, S., Z. A. Raza, M. I. Majeed, and T. Jan. 2018. Synthesis of zinc sulfide nanoparticles and their incorporation into poly(hydroxybutyrate) matrix in the formation of a novel nanocomposite. *Materials Research Express* 5 (5):055027. doi:10.1088/2053-1591/aac1f9.

Shamsudin, S. A., and J. Junas. 2018. Kajian terhadap sifat optik titik kuantum kadmium sulfida pada pelbagai nilai pH dan modifikasi permukaan dengan asid tioglikolik. *Sains Malaysiana* 47 (11):2841–9. doi:10.17576/jsm-2018-4711-27.

Sousa, D. M., L. C. Alves, A. Marques, G. Gaspar, J. C. Lima, and I. Ferreira. 2018. Facile microwave-assisted synthesis manganese doped zinc sulfide nanoparticles. *Scientific Reports* 8 (1):1–7. doi:10.1038/s41598-018-34268-z.

Teow Y. H., M. Shah, K. C. Ho, A. W. Mohammad. 2018. A study on membrane technology for surface water treatment: Synthesis, characterization and performance test. *Membrane Water Treatment* 2:69–77. doi:10.12989/mwt.2018.9.2.069.

Uma, B., T. N. Swaminathan, R. Radhakrishnan, D. M. Eckmann, and P. S. Ayyaswamy. 2011. Nanoparticle Brownian motion and hydrodynamic interactions in the presence of flow fields. *Physics of Fluids* 23 (7):73602–15. doi:10.1063/1.3611026.

Verheyen, E., J. P. Schillemans, M. van Wijk, M.-A. Demeniex, W. E. Hennink, and C. F. van Nostrum. 2011. Challenges for the effective molecular imprinting of proteins. *Biomaterials* 32 (11):3008–20. doi:10.1016/j.biomaterials.2011.01.007.

Wang, L., P. Wang, B. Huang, X. Ma, G. Wang, Y. Dai, X. Zhang, and X. Qin. 2017. Synthesis of Mn-doped ZnS microspheres with enhanced visible light photocatalytic activity. *Applied Surface Science* 391:557–64. doi:10.1016/j.apsusc.2016.06.159.

Wang, Z., R. Long, M. Peng, T. Li, and S. Shi. 2019. Molecularly imprinted polymers-coated CdTe quantum dots for highly sensitive and selective fluorescent determination of ferulic acid. *Journal of Analytical Methods in Chemistry* 2019:1–8. doi:10.1155/2019/1505878.

Wu, P., J. Zhang, S. Wang, A. Zhu, and X. Hou. 2014. Sensing during in situ growth of Mn-doped ZnS QDs: A phosphorescent sensor for detection of H2S in biological samples. *Chemistry* 20 (4):952–6. doi: 10.1002/chem.201303753.

Zhang, X., S. Yang, L. Sun, and A. Luo. 2016. Surface-imprinted polymer coating L -cysteine-capped ZnS quantum dots for target protein specific recognition. *Journal of Materials Science* 51 (12):6075–85. doi:10.1007/s10853-016-9914-7.

Zhang, X., S. Yang, R. Jiang, L. Sun, S. Pang, and A. Luo. 2018. Fluorescent molecularly imprinted membranes as biosensor for the detection of target protein. *Sensors and Actuators B: Chemical* 254: 1078–86. doi:10.1016/j.snb.2017.07.205.

Zhao, J. L., C. Zhao, Lan, and S. Zhao. 2016. Graphene quantum dots as effective probes for label-free fluorescence detection of dopamine. *Sensors and Actuators B: Chemical* 223:246–51. doi:10.1016/j.snb.2015.09.105.